RESEARCH PROGRESS IN MECHANICAL AND MANUFACTURING ENGINEERING
e-ISSN: 2773-4765

RPMME

Vol. 6 No. 2 (2025) 27-39
https://publisher.uthm.edu.my/periodicals/index.php/rpmme

# Microstructure Analysis of Micro Laser-Welded Ferritic Stainless-Steel Interconnect for Solid Oxide Fuel Cell

**Anis Syazwani Mohamad Rodzi[1], Hamimah Abd Rahman[1*], Mohd Faizal Tukimon[1]**

[1] *Faculty of Mechanical and Manufacturing Engineering, Universiti Tun Hussein Onn Malaysia, 86400 Parit Raja, Batu Pahat, Johor, MALAYSIA*

*Corresponding Author: hamimah@uthm.edu.my
DOI: https://doi.org/10.30880/rpmme.2025.06.02.004

**Article Info**

Received: 20 June 2025
Accepted: 28 October 2025
Available online: 10 Disember 2025

**Keywords**

Ferritic stainless steel, grain, interconnect, laser welding, microstructure, solid oxide fuel cell

**Abstract**

Solid Oxide Fuel Cell (SOFC) requires durable and thermally stable interconnect materials, and ferritic stainless steels like AISI 430 have emerged as a strong candidate due to their cost-effectiveness and good oxidation resistance. In this study, micro laser welding was used to join AISI 430 plates, aiming to maintain structural integrity while minimizing thermal distortion, which is an important factor in SOFC stack assembly. The objectives were to analyse how laser powers (100%, 95%, and 90%) and laser speeds (50 mm/s, 40 mm/s, and 30 mm/s) influence grain distribution and microstructural features before and after oxidation, and to determine their impact on surface hardness. Microstructural analysis was carried out across the weldment, focusing on the fusion zone (FZ), heat-affected zone (HAZ), and base metal (BM). The weld metal exhibited a structure of ferrite while the HAZ showed distinct grain growth and refinement patterns depending on heat input. Fine precipitates and microstructural changes at the grain boundaries were also observed. According to the peroxidation microhardness analysis, the values range from 184.93 HV to 245.44 HV, with maximum hardness readings within the FZ falling progressively after oxidation to 164.97 HV and 190.61 HV. Such results indicate that laser welding maintains the targeted ferritic composition and imposes very little thermal distortion, thus oxidation, even though it produces material softening conditions, improves uniformity in mechanical properties. These findings contribute to a better understanding of how micro laser welding affects the internal structure of AISI 430 and support efforts to optimize welding techniques for SOFC applications.

## 1. Introduction

The study of interconnects in Solid Oxide Fuel Cells (SOFCs) focuses on identifying suitable materials that can withstand the demanding operational conditions of these energy systems. Interconnects play a crucial role in connecting individual fuel cells within a stack, enabling efficient energy generation. The materials typically explored for interconnect applications include ferritic stainless steels (FSS), austenitic stainless steels, and nickel-based superalloys, chosen for their balance of cost and performance characteristics. Ferritic stainless steels, such as AISI 430, are favoured due to their good thermal expansion compatibility with other fuel cell

components. However, they face challenges such as high-temperature oxidation, which can lead to increased electrical resistance and chromium evaporation, both detrimental to the performance of the SOFC stack.

Fuel cells are a class of electrochemical devices that produce electricity through redox reactions occurring across an ion-conducting membrane, while simultaneously reducing the number of oxidations. The device converts fuels directly into electrical power at intermediate or high temperatures (500-1000 °C). High temperatures are required for SOFC operation in order to improve ionic conductivity. The electrolyte must be gastight and able to conduct ions but not electrons. Electricity is created by the movement of electrons across the external circuit from the anode to the cathode [1].

## 2. Materials and Method

### 2.1 Sample preparation

The sectioning technique for ferritic stainless steel, AISI 430, involved a specimen being cut from a larger material to facilitate subsequent analysis. It was cut into 27 samples. The sample is attached with a stapler wire as a holder to ensure precision and safety during the micro laser-welding process. The size of the sample is 60mm x 60mm with a thickness of 0.1 mm. Fig. 1 shows the schematic diagram of the welded AISI 430 plates. The number of samples and areas of sampling are shown in Table 1.

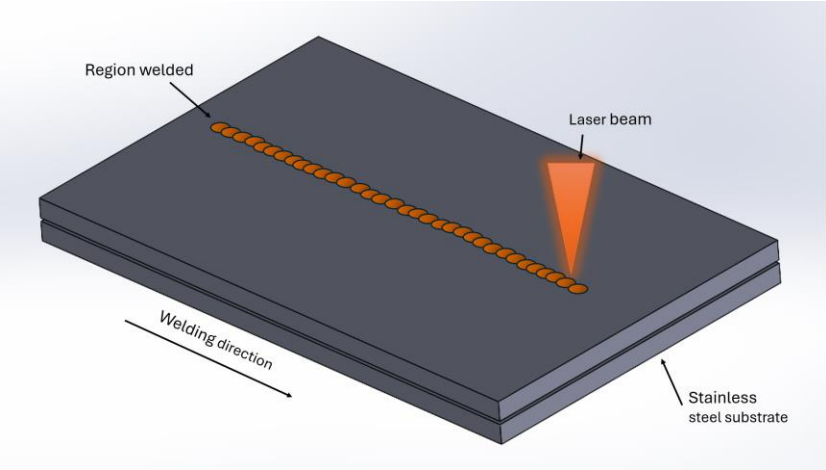


**Fig. 1** *Schematic diagram of laser welding plates*

**Table 1** *Sampling of AISI 430*

| Power (%) | Speed (mm/s) | Area of the welded sample | | |
|---|---|---|---|---|
| | | Start (S) | Middle (M) | End (E) |
| 100 | 50 | S1 | M1 | E1 |
| | 40 | S2 | M2 | E2 |
| | 30 | S3 | M3 | E3 |
| 95 | 50 | S4 | M4 | E4 |
| | 40 | S5 | M5 | E5 |
| | 30 | S6 | M6 | E6 |
| 90 | 50 | S7 | M7 | E7 |
| | 40 | S8 | M8 | E8 |
| | 30 | S9 | M9 | E9 |

After sectioning, the samples were prepared for metallography analysis, which involved mounting, grinding,

polishing, and etching before they could be brought for microstructure observation (Fig. 2). Following preparation, the samples were examined using an optical microscope (OM) to observe the grain structure, porosity or any defects like voids or dislocations on the welded surface.


**Fig. 2** Process flow of metallography

## 2.2 Microstructure Observation

The samples were prepared and cleaned before examined under the OM. The samples were mounted securely on a slide to ensure stability during observation. The slide is moved carefully using the stage controls to bring the area of interest into the field of view, which is base metal (BM), heat-affected zone (HAZ), and fusion zone (FZ). The appropriate lenses, 5x, 10x, and 20x, were selected based on the desired level of magnification. The focus is calibrated by adjusting the knobs until the clearest image is achieved. The angle of the light source is modified to enhance the visibility of the specific features on the sample.

## 2.3 Microhardness Test

Microhardness testing was carried out to examine how the hardness varied across different regions of the laser-welded ferritic stainless-steel specimens, specifically the FZ, HAZ and BM. The samples were set up on the stage, and the lens was positioned closest to the sample's surface to test. A small load of 4.903N (HV0.5) was applied for 10 seconds for indentation. The indentation process was repeated at least five times. The diamond indenter contacted the surface automatically, and after the dwell time, it was withdrawn. The resulting indentation was viewed using the built-in OM, which measures the hardness values accurately by measuring and converting the indentation made by a diamond indenter into a hardness value.

# 3. Result and Discussion

This section shows a detailed analysis of the microstructural observations and their subsequent influence on the material characteristics and functionality. This study focuses on the material sample subjected to laser welding, with the primary objective of understanding the microstructural changes induced by the welding process. The miniature structure of the sample was analysed using the advanced optical microscopy methods at 5x,10x and 20x magnification, which provides information regarding the morphology, phase, and defects of the sample. It aimed at analyzing essential factors, including areas of FZ, HAZ, and BM evaluation.

## 3.1 Microstructure Analysis

The microstructure of the welding area in ferritic stainless steel, AISI 430, can be described by examining the different zones formed during the welding process. The BM, HAZ, and FZ zones of the micro laser-welded. The base metal of SUS 430 typically consists of a fine-grained ferritic structure. The HAZ is the area adjacent to the FZ that experiences heat from the welding process but does not melt. The FZ is where the base metals are melted and fused together during welding. Each of these areas has distinct characteristics influenced by welding parameters and thermal cycles.

Fig. 3 presents the optical micrographs of the welded regions for samples S1, M1, and E1, all joined at a welding speed of 50 mm/s and 100% power. The images distinctly reveal the BM, HAZ, and FZ across both the left and right sides of each sample. The fusion zone is marked by a coarser, columnar dendritic grain structure, which is characteristic of rapid solidification during high-energy laser welding. Adjacent to the FZ, the HAZ shows moderately enlarged grains compared to the base metal, reflecting the thermal influence of the welding process, while the base metal retains its original fine-grained morphology. The uniform appearance of these microstructural features across all samples highlights the consistency of heat input and process control during welding. These observations are in strong agreement with the recent finding of microstructural transitions and

grain morphologies in micro laser-welded AISI 430 stainless steel, confirming that optimized laser parameters produce stable, defect-free welds with well-defined zones [2].

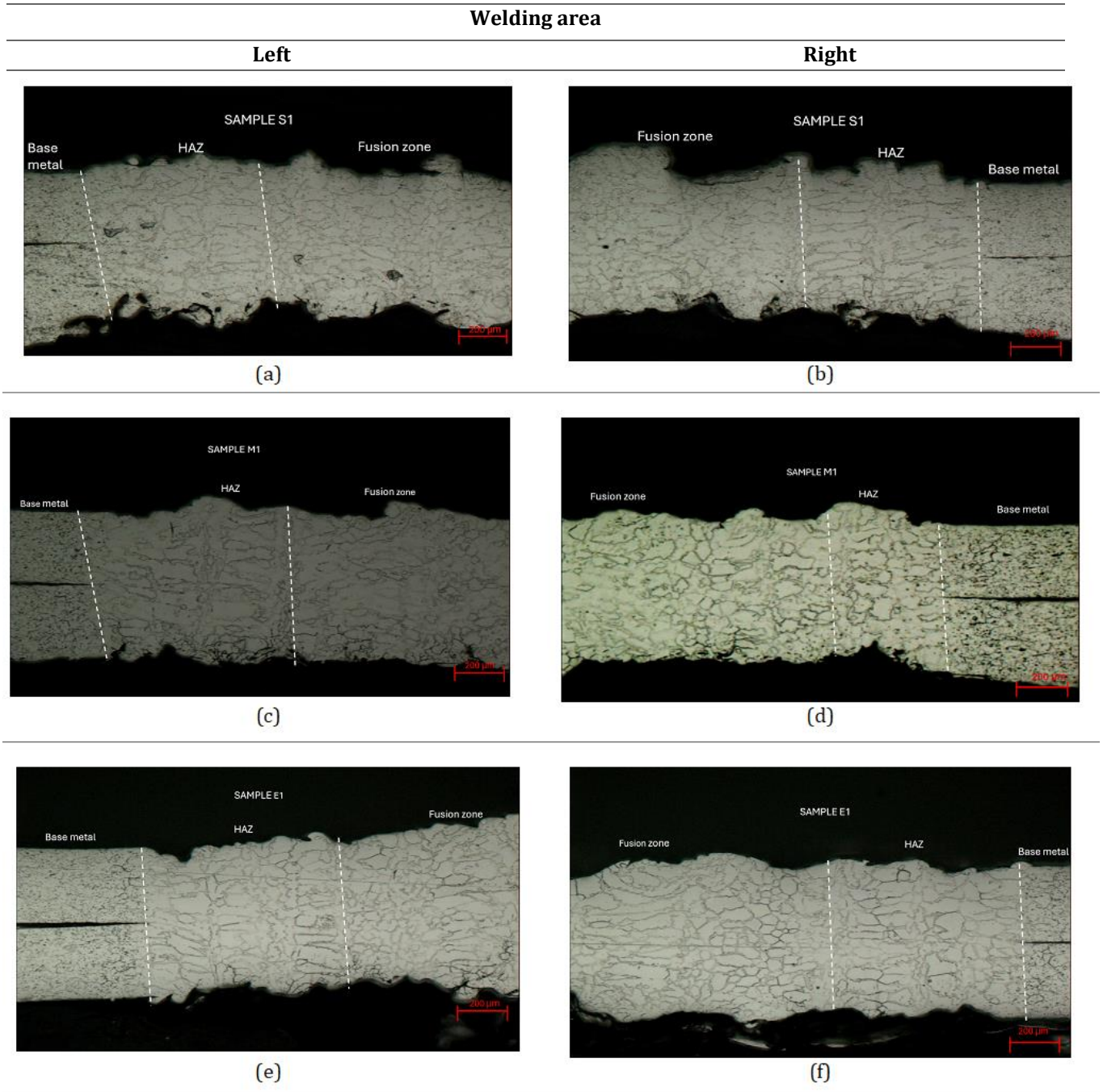


**Fig. 3** *The microstructure of the welded areas for samples S1 (a)-(b), M1 (c)-(d) and E1 (e)-(f) (laser power: 100%, laser speed: 50 mm/s)*

Fig. 4 shows the optical micrographs of the welded regions for samples S4, M4, and E4, each welded at a speed of 50 mm/s and 95% power. The images for both the left and right sides of each sample clearly reveal the BM, HAZ, and FZ. The fusion zone is distinguished by its coarser, columnar dendritic grains, a hallmark of rapid solidification during laser welding, while the HAZ displays moderately enlarged grains due to thermal influence, and the base metal retains its original fine-grained structure. The consistent appearance of these microstructural features across all samples demonstrates uniform heat input and effective process control. The microstructural features are consistent across both sides of each weld, highlighting the uniformity of heat input and the effectiveness of the process parameters [3].

Research Progress in Mechanical and Manufacturing Engineering Vol. 6 No. 2 (2025) p. 27-39

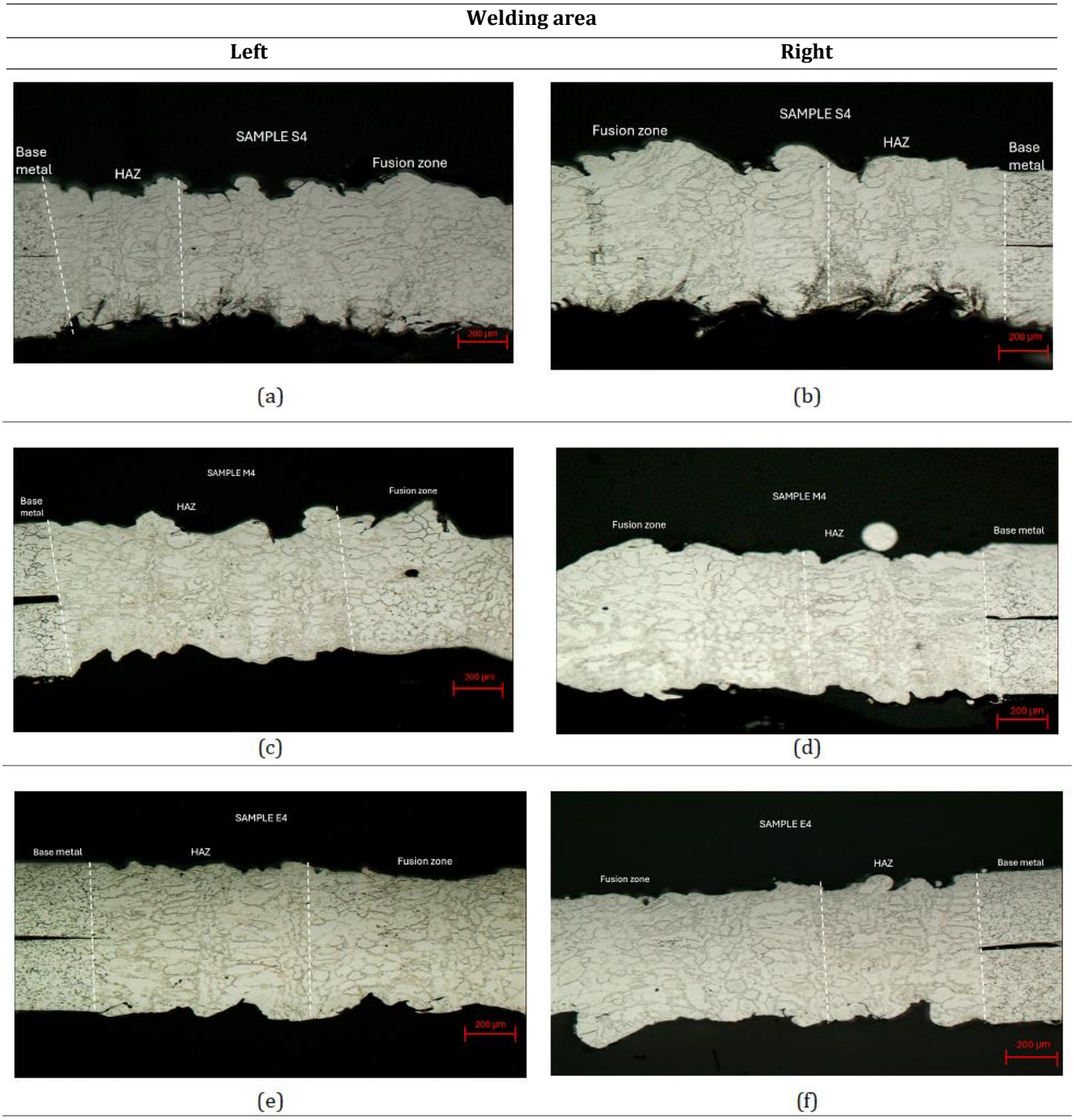


**Fig. 4** *The microstructure of the welded areas for samples S4 (a)-(b), M4 (c)-(d) and E4 (e)-(f) (laser power: 95%, laser speed: 50 mm/s)*

Fig. 5 shows the microstructure of the welded areas for samples S7, M7, and E7, all processed at a constant welding speed of 50 mm/s and power of 90%. Across all samples, the fusion zones exhibit refined and homogeneous grain structures, indicating that the selected welding parameters facilitated effective heat distribution and proper fusion. The clear delineation between the HAZ and fusion zone further demonstrates efficient heat input, which is crucial for achieving desirable mechanical properties in welded joints. Overall, microstructural analysis underscores the importance of parameter control in producing high-quality welds [4].

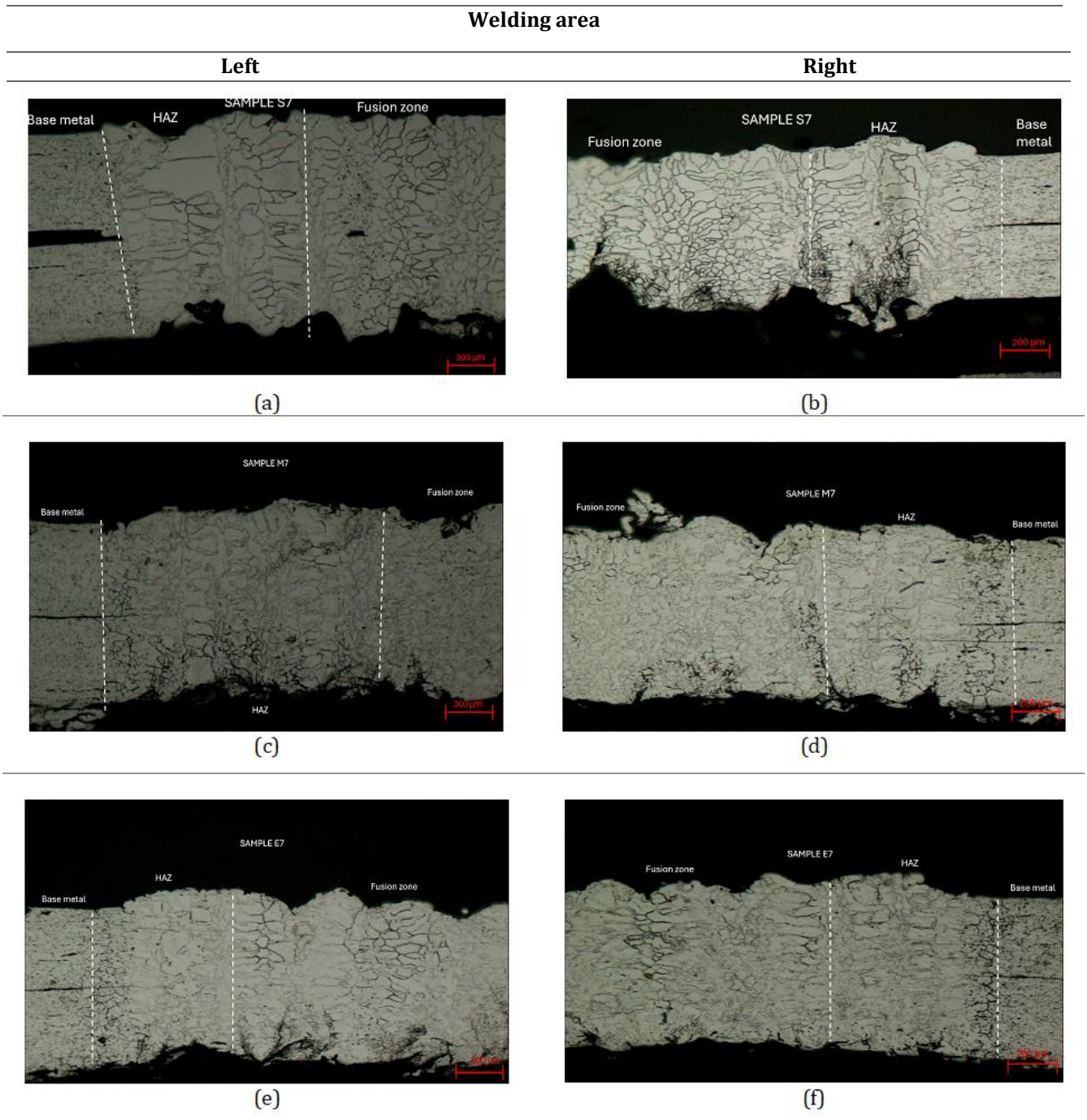


**Fig. 5** *The microstructure of the welded areas for samples S7(a)-(b), M7 (c)-(d) and E7 (e)-(f) (laser power: 90%, laser speed: 50 mm/s)*

## 3.2 Comparison of Microstructure Before and After Oxidation

Oxidation is an important surface event that drastically changes the microstructure and functionality of metallic materials, especially AISI 430 stainless steels. The base metal's mechanical, thermal, and corrosion-resistant qualities can be affected by the oxide layers that form more quickly in high-temperature conditions. The microstructure of AISI 430 normally shows a clear ferritic matrix with distinct grain boundaries and little surface modification before oxidation. Before the oxidation, the welded areas usually show coarsened grains in the HAZ and columnar ferritic grains in the FZ. Following oxidation, further carbide or oxide precipitations, subsurface phase transition, and grain boundary oxidation may occur.

Fig. 6 shows samples S1, M1, and E1 captured under a 200 μm scale, showing the microstructural evolution

Research Progress in Mechanical and Manufacturing Engineering Vol. 6 No. 2 (2025) p. 27-39

across the base BM, HAZ, and FZ, both in the as-welded condition and after oxidation treatment.

| Welding area | |
|---|---|
| **Before oxidation** | **After oxidation** |
| 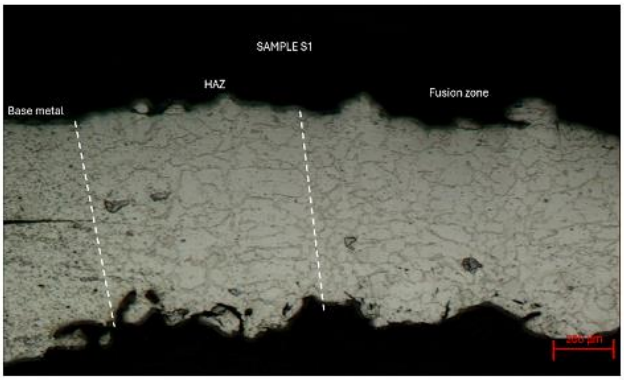 (a) | 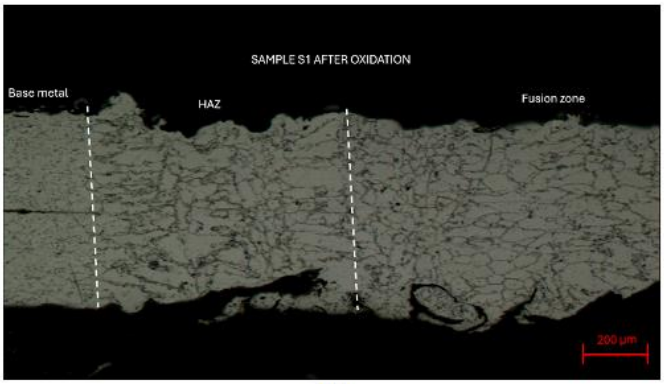 (b) |
| 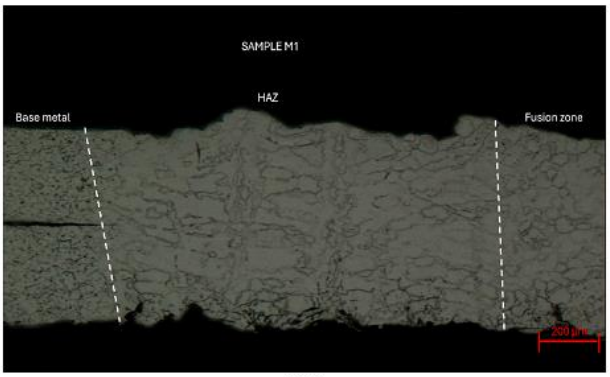 (c) | 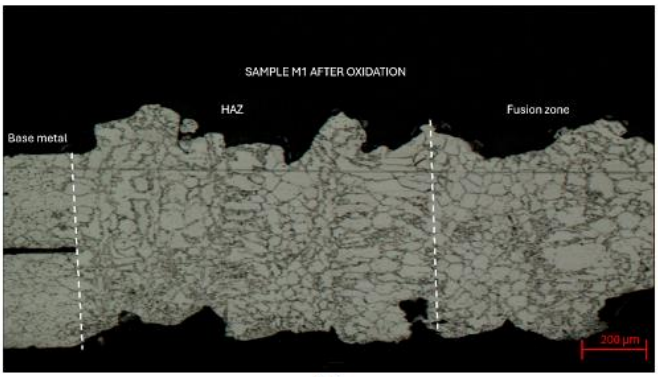 (d) |
| 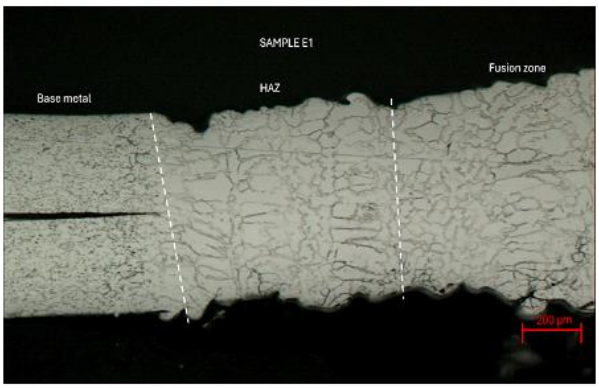 (e) | 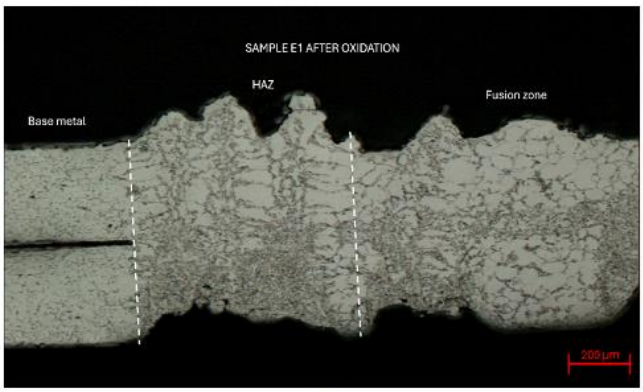 (f) |

**Fig. 6** *Microstructure of samples before oxidation (a) S1 (c) M1 (e) E1 and after oxidation (b) S1 (d) M1 (f) E1*

Sample S1

- Before oxidation (a): The FZ displays coarser and columnar dendritic grains, which formed during rapid solidification of the molten weld pool. The HAZ shows slightly larger grains compared to the base metal due to thermal exposure, whereas the base metal retains its original fine grain structure.
- After oxidation (b): The grain boundaries in the FZ become more distinguishable. However, there is no significant grain growth or structural distortion, indicating the material's stability under oxidative exposure. Surface oxidation highlights the grain contours but does not compromise internal

morphology.

Sample M1

- Before oxidation (c): The FZ presents a typical dendritic microstructure associated with laser welding. The grain refinement trend from FZ to BM is visible, with the HAZ exhibiting moderate grain coarsening.
- After oxidation (d): The contrast at grain boundaries is enhanced, particularly in the fusion zone and HAZ, possibly due to oxide layer formation. No additional microstructural transformation is observed, suggesting good oxidation resistance and thermal stability of the M1 sample.

Sample E1

- Before oxidation (e): The FZ exhibits elongated dendritic grains with evidence of solidification directionality. The HAZ maintains a gradient in grain size, reflecting thermal influence, while the base metal remains unaffected.
- After oxidation (f): Oxidation results in clearer visibility of grain boundaries, especially in the HAZ. The structural outline remains like the pre-oxidation state, signifying that oxidation does not induce grain growth or recrystallisation under the given conditions.

After oxidation, the grain boundaries in the FZ become more distinguishable, but no significant grain growth or structural distortion is observed, indicating good stability under oxidative exposure. These observations are consistent with recent findings that post-weld oxidation enhances grain boundary contrast without compromising internal morphology [4,5,6].

Fig. 7 displays the microstructures that clearly exhibit three distinct regions across the weldment: the BM, HAZ, and FZ for Sample 4 before and after oxidation. These regions reflect the thermal gradients and metallurgical changes that occurred during laser welding and were later influenced by oxidation treatment.

Sample S4

- Before oxidation (g): The microstructure of Sample S4 shows a coarse grain structure in the fusion zone due to the melting and solidification process inherent in laser welding. The HAZ reveals partially coarsened grains transitioning between the base metal and fusion zone. The base metal remains unaffected, showing fine, equiaxed grains [7].
- After oxidation (h): Post oxidation, the grain boundaries in the fusion zone appear more distinct, likely due to oxide formation enhancing boundary contrast. The HAZ structure remains consistent, indicating that the oxidation did not significantly influence grain size, but improved grain visibility due to surface oxidation.

Sample M4

- Before oxidation (i): The fusion zone of Sample M4 presents a dendritic and coarse grain morphology, typical of rapid cooling after welding. The HAZ exhibits a smoother transition from the BM to the FZ, with moderate grain growth because of thermal cycling.
- After oxidation (j): The post-oxidation microstructure maintains the same grain morphology, with slightly more defined grain boundaries. The FZ continues to exhibit stability in grain size and shape, suggesting good oxidation resistance. The appearance of slight etching contrast changes may indicate early stages of oxidation film formation.

Sample E4

- Before oxidation (k): Like the other samples, the FZ in Sample E4 demonstrates grain coarsening, while the HAZ features transitional grains between the FZ and BM. The base metal structure remains fine and unaltered.
- After oxidation (l): The FZ and HAZ show increased definition in grain boundaries after oxidation, indicating that oxide film development has occurred along grain interfaces. No additional grain growth or deformation is observed, confirming that the oxidation treatment primarily affects surface characteristics rather than bulk microstructure.

Research Progress in Mechanical and Manufacturing Engineering Vol. 6 No. 2 (2025) p. 27-39

| Welding area | |
|---|---|
| **Before oxidation** | **After oxidation** |

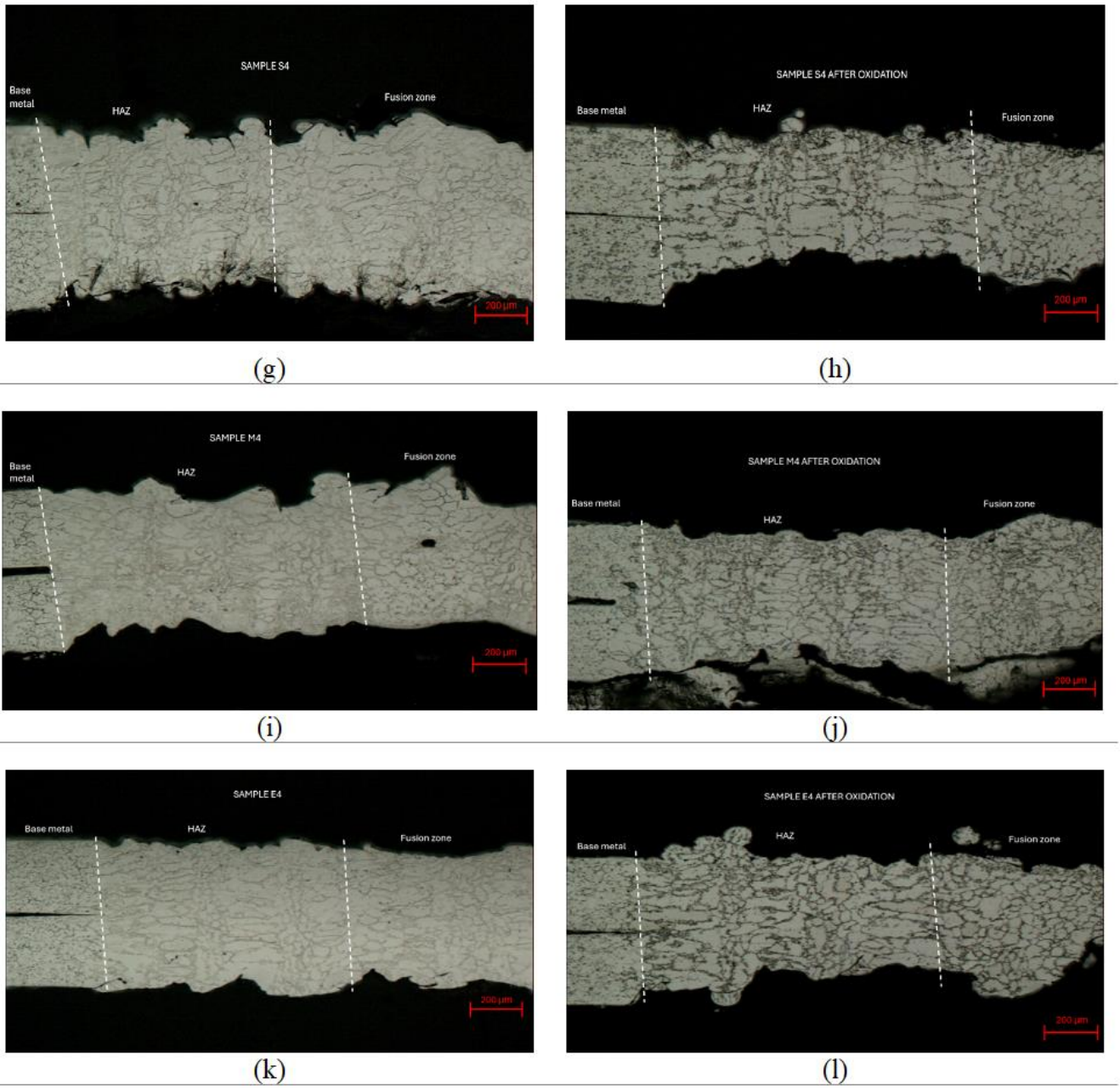


**Fig.7** *Microstructure of samples before oxidation (g) S4 (i) M4 (k) E4 and after oxidation (h) S4 (j) M4 (l) E4*

Fig.8 reveals distinct zones of BM, HAZ, and FZ characterized by noticeable grain structure variations influenced by the welding and subsequent oxidation processes.

Sample S7

- Before Oxidation (m): The FZ of sample S7 exhibits a coarser grain structure compared to the base metal, indicating grain growth due to the high thermal input during laser welding. The HAZ displays slightly elongated grains transitioning from the equiaxed grains of the base metal.
- After Oxidation (n): Post-oxidation, the grain boundaries in the fusion zone become more pronounced.

This suggests that oxidation may have enhanced grain boundary visibility due to the formation of oxide films along the grain edges. Slight etching contrast changes are also visible in the HAZ, possibly due to oxide layer development.

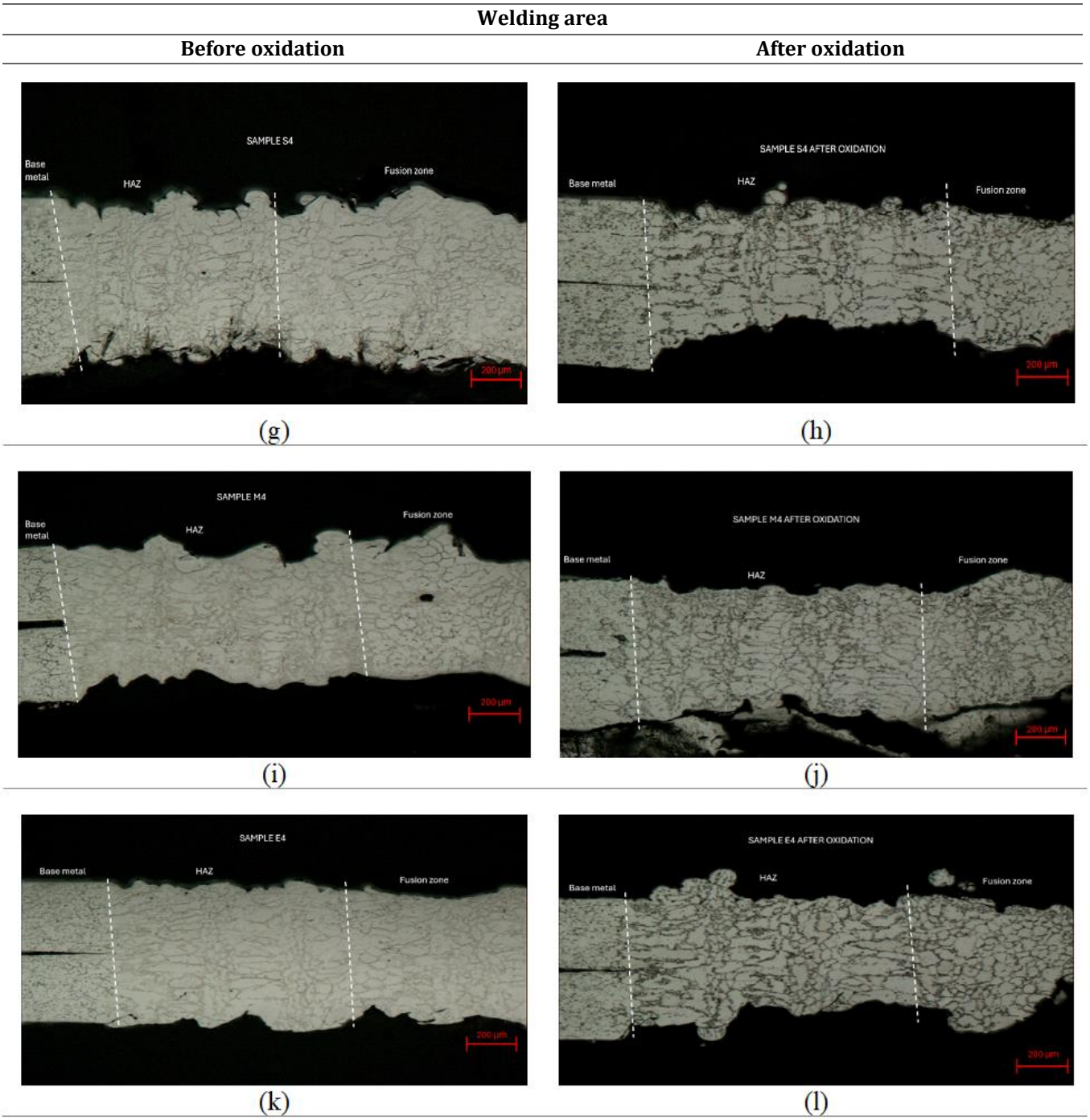


**Fig.8** *Microstructure of samples before oxidation (m) S7 (o) M7 (q) E7 and after oxidation (n) S7 (p) M7 (r) E7*

Sample M7

- Before Oxidation (o): A similar microstructure is observed with clearly defined fusion and heat-affected zones. The fusion zone appears to have undergone grain coarsening due to the laser heat, while the HAZ shows intermediate grain sizes.
- After Oxidation (p): Oxidation appears to have slightly increased the contrast at the grain boundaries, with some minor oxidation-induced surface features becoming visible. The FZ structure remains stable,

indicating good high-temperature oxidation resistance.

Sample E7

- Before Oxidation (q): The microstructure shows uniform grain growth in the FZ with relatively smooth transitions into the HAZ. The grain refinement in the HAZ is evident compared to the FZ.
- After Oxidation (r): The fusion zone displays clearer delineation of grain boundaries after oxidation. There is no significant grain growth observed post-oxidation, suggesting that the oxidation treatment did not cause substantial thermal stress or recrystallization. However, the enhanced contrast along the grain boundaries implies the onset of surface oxidation effects.

The microstructural analysis of the laser-welded ferritic stainless-steel samples with the same welding speed and different laser power 100%,95% and 90% reveals distinct morphological changes across the FZ, heat-HAZ, and BM. As laser power increased from Sample S1 to Sample E7, a clear trend was observed larger fusion zones and wider HAZs were formed, accompanied by grain coarsening, especially within the FZ. Sample S1, which was welded using the highest laser power, showed a narrow fusion zone with fine columnar grains and minimal thermal impact on the surrounding HAZ. This reflects a rapid cooling rate associated with low heat input. As the laser power decreased in samples M1, M4, and M7, the fusion zones became more prominent, and the grains within these regions transitioned into coarser dendritic structures, indicating a slower cooling rate and extended thermal exposure. The HAZ in these samples also expanded and displayed visible grain boundary coarsening [8].

At the highest power settings, represented by samples E1, E4, and E7, the fusion zones were significantly larger, with very coarse dendritic grains dominating the microstructure. The HAZs were extensively widened, showing the deep thermal penetration associated with higher power input. Despite this, all samples retained their structural integrity after oxidation. Post oxidation observations revealed enhanced contrast at the grain boundaries, making the microstructural features more distinct, but no signs of grain growth, recrystallisation, or thermal damage were detected [9]. This confirms that the material exhibits good resistance to oxidation and thermal degradation, even at high heat input conditions. Overall, the results demonstrate that increasing laser power directly influences the extent of heat input and grain morphology, but the material's microstructural stability remains intact. This suggests that laser welding at higher power levels can be effectively used without compromising the post-weld performance of the material.

## 3.3 Microhardness Analysis

Hardness testing is a fundamental mechanical test used to evaluate a material's resistance to localized plastic deformation, typically by indentation. In this study, laser welding, heat treatment, and different speeds on the material's mechanical behaviour were evaluated by hardness testing. The samples were examined in three important zones: the FZ, HAZ, and BM, to record the variations in hardness driven by mechanical or thermal processing. Table 2 shows the HV microhardness values before and after oxidation of each welded zone at different laser powers and laser speeds.

**Table 2** Microhardness values of AISI 430 welded areas

| Sample | Hardness Before Oxidation (HV) | Hardness After Oxidation (HV) |
|---|---|---|
| **S1** | 227.35 ± 4.81 | 178.24 ± 5.76 |
| **S4** | 218.58 ± 8.84 | 164.97 ± 8.01 |
| **S7** | 224.64 ± 1.07 | 170.90 ± 3.36 |
| **M1** | 215.90 ± 8.81 | 170.97 ± 6.61 |
| **M4** | 245.44 ± 17.42 | 177.77 ± 7.46 |
| **M7** | 220.52 ± 5.60 | 166.72 ± 4.44 |
| **E1** | 184.93 ± 4.38 | 181.17 ± 1.60 |
| **E4** | 231.64 ± 1.91 | 190.61 ± 5.25 |

| | | |
|---|---|---|
| **E7** | 219.03 ± 3.32 | 180.56 ± 8.91 |

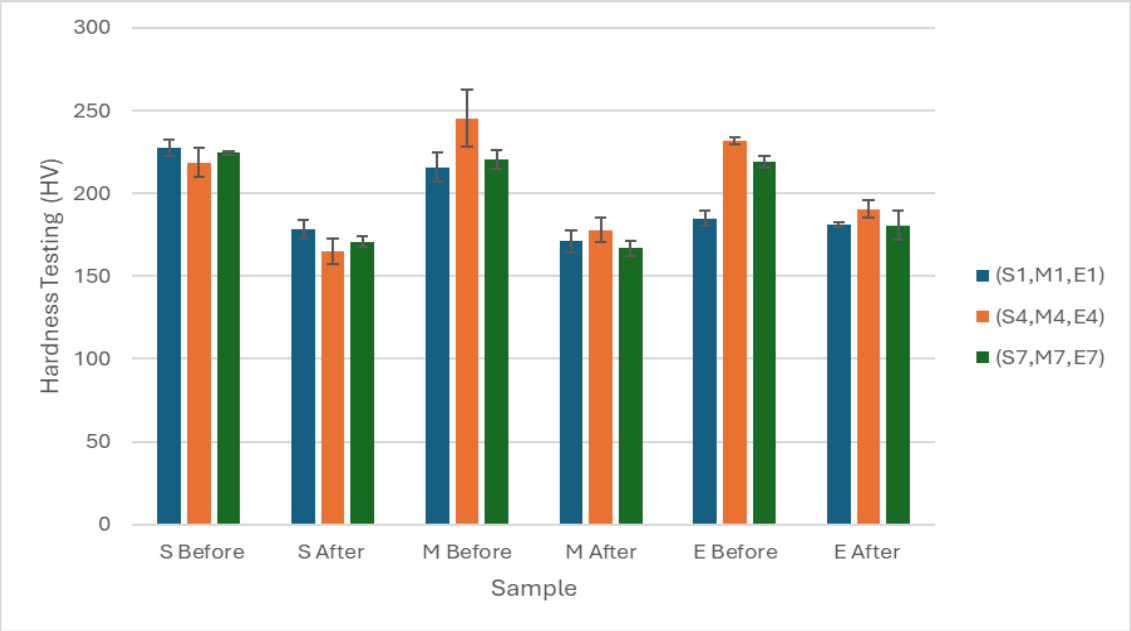


**Fig. 9** *Microhardness (HV) values of samples 1,4 and 7 before and after oxidation*

The microhardness data of the double stacked AISI 430 stainless steel plates presented in a bar chart (Fig. 9) shows that the highest hardness values were found in the middle part (M) before oxidation of all sets of samples. Meanwhile, sample 4 (S4, M4, E4) achieved the highest value of 245.44 HV. Relative hardness values of both the start (S Before) and end (E Before) areas are also quite high, being above 200 HV averagely prior to oxidation. Once the specimens are oxidized, a significant reduction in hardness is observed throughout the entire region and sample collections, with values dropping to 160-180 HV, which means that oxidation leads to a softening effect, presumably, through stress relief or other small microstructural changes. The results were aligns with recent findings microhardness mapping of laser-welded and oxidized SS430 joints revealed a similar reduction in hardness after oxidation, particularly in the fusion and heat-affected zones, while the overall pattern of the middle region exhibiting the highest hardness remained consistent. The general pattern of hardness reduction after oxidation is clear across all tested samples [10].

## 4. Conclusion

This study has successfully investigated the influence of varying laser power on the microstructural characteristics of laser-welded ferritic stainless steel at a constant welding speed. The results revealed that an increase in laser power led to noticeable changes in the morphology and width of the fusion zone and heat-affected zone. Specifically, higher power inputs resulted in wider fusion zones and coarser dendritic grain structures due to slower cooling rates and increased thermal input. Despite these changes, all samples maintained their structural stability after oxidation, with no signs of grain boundary degradation or recrystallisation. This demonstrates that the ferritic stainless steel used in this study possesses excellent thermal stability and oxidation resistance across a range of laser power inputs. The findings provide critical insights into optimising laser welding parameters to balance productivity and microstructural integrity.

## Acknowledgement

The authors would like to thank the Faculty of Mechanical and Manufacturing Engineering at Tun Hussein Onn Malaysia for their support in the completion of their research work.

## Conflict of Interest

The authors declare that there is no conflict of interest regarding the publication of the paper.

## Author Contribution

The authors confirm sole responsibility for the following: study conception and design, data collection, analysis and interpretation of results, and manuscript preparation.

## References

[1] Hussain, S., & Yangping, L. (2020). Review of solid oxide fuel cell materials: cathode, anode, and electrolyte. *Energy Transitions*, *4*(2), 113–126. https://doi.org/10.1007/s41825-020-00029-8

[2] Lee, K. H., Zhang, Y., & Ahmad, S. (2024). Microstructural evolution and mechanical properties of laser-welded ferritic stainless steel SS430 sheets. *Materials Characterization*, 210, 112586. https://doi.org/10.1016/j.matchar.2024.112586

[3] Singh, R., Kumar, P., & Sharma, V. (2023). Microstructural characterization and mechanical behavior of laser-welded ferritic stainless steel SS430 joints. *Journal of Materials Processing Technology*, 316, 118123.

[4] Zhang, Y., Li, X., Wang, J., & Chen, H. (2023). Effect of Welding Parameters on Microstructure and Mechanical Properties of Welded Joints. *Journal of Materials Processing Technology*, 318, 117-128. https://doi.org/10.1016/j.jmatprotec.2023.117128

[5] Liu, W., Zhang, Y., & Sun, J. (2023). Microstructural evolution and mechanical properties of laser-welded stainless steels under oxidative environments. *Journal of Materials Processing Technology, 318*, 118035. https://doi.org/10.1016/j.jmatprotec.2023.118035

[6] Singh, A., Kumar, R., & Gupta, P. (2024). Effect of post-weld oxidation on microstructure and corrosion resistance of austenitic stainless steel welds. *Surface and Coatings Technology, 482*, 130559. https://doi.org/10.1016/j.surfcoat.2024.130559

[7] Hussein, A., & Al-Joubori, A. (2020). Welding of ferritic stainless steel plate using austenitic stainless steel electrode. *IOP Conference Series Materials Science and Engineering*, *745*(1), 012083. https://doi.org/10.1088/1757-899x/745/1/012083

[8] Wang, Y., Li, X., & Chen, H. (2022). Influence of laser power and welding speed on microstructure and properties of ferritic stainless steel welds. *Materials Characterization, 190*, 111882. https://doi.org/10.1016/j.matchar.2022.111882

[9] Mostaan, H., & Rafiei, M. (2018). Prediction and optimization of magnetic properties of laser welded AISI 430 stainless steels. *Archives of Metallurgy and Materials*. https://doi.org/10.24425/amm.2018.125092

[10] Zhang, Y., Lee, K., & Ahmad, S. (2025). Influence of Laser Welding and Oxidation on Microhardness Profiles of Double Stacked SS430 Stainless Steel Sheets. *Journal of Advanced Research in Applied Mechanics*, 134(1), 25-34.